James A. Poulter^{1,3}, Steven J. Brookes^{2,3}, Roger C. Shore², Claire E. L. Smith¹, Layal

Abi Farraj¹, Jennifer Kirkham², Chris F. Inglehearn¹ and Alan J. Mighell^{1,2,*}

¹Leeds Institutes of Molecular Medicine, University of Leeds, Leeds, LS9 7TF, UK

²School of Dentistry, University of Leeds, Leeds, LS2 9LU, UK

^{*}To whom correspondence should be addressed. Dr A.J. Mighell, Department of Oral

Medicine, School of Dentistry, University of Leeds, Clarendon Way, Leeds, LS2

9LU, UK. Tel: +44 1133435688; Fax: +44 1133436165; Email:

A.J.Mighell@leeds.ac.uk

³These authors contributed equally to this study.

1

Abstract

We identified a family in which pitted hypomineralised AI with premature enamel failure segregated in an autosomal recessive fashion. Whole exome sequencing revealed a missense mutation (c.586C>A, p.P196T) in the I-domain of integrin- β 6 (ITGB6), which is consistently predicted to be pathogenic by all available programmes and is the only variant that segregates with the disease phenotype. Furthermore, a recent study revealed that mice lacking a functional allele of Itgb6 display a hypomaturation AI phenotype. Phenotypic characterisation of affected human teeth in this study showed areas of abnormal prismatic organisation, areas of low mineral density and severe abnormal surface pitting in the tooth's coronal portion. We suggest that the pathogenesis of this form of AI may be due to ineffective ligand binding of ITGB6 resulting in either compromised cell-matrix interaction or compromised ITGB6 activation of TGF β impacting indirectly on ameloblast-ameloblast interactions and proteolytic processing of extracellular matrix proteins via MMP20. This study adds to the list of genes mutated in AI and further highlights the importance of cell-matrix interactions during enamel formation.

Introduction

Enamel is the hardest human tissue and when formed correctly has the capacity to remain functional in to very old age. Amelogenesis Imperfecta (AI) is the collective term for a heterogeneous group of conditions characterised by genetically determined defects in tooth enamel biomineralisation that lead to premature clinical failure. Typically, all teeth of the primary and secondary dentitions are affected, with variations in phenotype being influenced by the underlying genotypes (1). The impact of AI on affected individuals, their families and those providing longitudinal care is considerable (2).

Amelogenesis is a stepwise process conserved between species (3), yet the precise mechanisms underlying each phase are not well understood. The basic unit of enamel structure is the prism (or rod), with each prism representing a bundle of nanocrystals of calcium hydroxyapatite mineral ($Ca_{10}[PO_4]_6[OH]_2$) (HAP). The physical properties of mature enamel are a result of its high mineral content and the complex, though ordered, spatial inter-relationship and orientation of the enamel prisms. For correct enamel formation to occur, ameloblasts must undergo four main stages: pre-secretory, secretory, transition and maturation (4). Briefly, ameloblasts grow in length and secrete an enamel matrix at their apical surface which forms the initial layer of aprismatic enamel. As the ameloblasts retreat away from the dentine they lay down an extracellular matrix within which the hydroxyapatite crystals begin to form. Each enamel prism reflects the migration path of an ameloblast, which is not straight but includes several changes in direction. The highly organised interlocking prismatic pattern resulting from the concerted movement of ameloblast cohorts provides the structure that is key to the physical strength of the final enamel (5). During the maturation stage, ameloblast-mediated proteolytic destruction and removal (via secretion of the protease KLK4) of organic material from the matrix and ameloblastmediated ion exchange is required for HAP crystals to grow in both thickness and width, until almost the entire tissue volume is occluded by mineral. By the end of the maturation stage, the newly formed enamel contains a mineral content of approximately 95% (by weight), (6), but due to the loss of cells from the crown surface on tooth eruption, it is without capacity for cellular repair.

AI can be subclassified on the basis of the volume of enamel matrix formed and its subsequent mineralisation. Prior to tooth eruption hypomineralised AI has a near normal enamel matrix volume that is not normally mineralised. Within the spectrum of hypomineralised AI there are two subtypes that typify the two extremes; hypocalcified and hypomaturation AI. In hypocalcified AI the enamel may be so soft that it can be scraped away by hand, whereas in hypomaturation AI the enamel is hard yet brittle and prone to fracture off. By contrast, in hypoplastic AI there is failure of enamel matrix formation. In its most extreme form a very thin layer of enamel, which may be hard or soft, covers the underlying dentine. As such, the tooth crowns have a markedly reduced enamel volume and an abnormal morphology clinically. Focal hypoplasia in the form of pits or grooves may occur within hypomineralised AI reflecting localised areas where enamel matrix formation has been incomplete.

Insight into enamel biomineralisation has been gained from identification of AIcausing mutations in genes encoding enamel matrix proteins (*AMELX*, MIM 30039; *ENAM*, MIM 606585), enamel matrix proteolytic enzymes (*KLK4*, MIM 603767; *MMP20*, MIM 604629), an ion transporter (*SLC24A4*, MIM 609840) and a putative crystal nucleator (*C4orf26*, MIM614829) (7-12). However, the identification of AIcausing mutations in *FAM83H* (MIM 611927) and *WDR72* (MIM 613214), which are of unknown functions, shows that much remains to be understood (13, 14).

Mutations in genes with an important role in cell-cell and cell-matrix adhesion, such as *ITGB4* (MIM 147557) and *LAMB3* (MIM 150310) have been identified in patients with isolated and syndromic AI (15-17). The finding that mutations in these genes, encoding integrins and laminins, cause AI, indicates that cell-cell and cell-matrix interactions play a vital role in amelogenesis. Recently, an *Integrin-\beta 6 (Itgb6*) null mouse was described with a hypomaturation AI phenotype (18), but to-date no human mutations have been identified in this gene as a cause of AI.

Here we report findings from a consanguineous family with autosomal recessive pitted hypomineralised AI. We show that a missense mutation of a highly conserved residue in ITGB6 is the cause of the condition in this family and that the enamel phenotype is similar to that described for the *Itgb6*-null model except that prism organisation is not completely lost in the human case. Based upon our detailed phenotyping and recently published data of others we suggest a potential pathogenic mechanism for AI in these patients based on ITGB6 activation of TGFβ and subsequent MMP20 activation via Runx2.

Results

Dental phenotype and SNP mapping.

We identified a consanguineous family (AI-23) living locally, but originating from Pakistan, in which pitted hypomineralised AI segregates with an autosomal recessive mode of inheritance in the absence of any other co-segregating diseases (Fig. 1). Affected individuals presented with poor dental aesthetics and associated pain, for example on eating or drinking.

To identify the genetic basis of AI in this family, individuals V:3 and V:5 were genotyped using Affymetrix 6.0 SNP microarrays and shared regions of homozygosity were identified using AutoSNPa (19). Six regions of homozygosity spanning approximately 73 Mb were identified (Table 1), none of which overlapped with previously published AI loci. We therefore decided to use whole exome sequencing to identify the cause of disease in this family.

Whole exome and Sanger sequencing

Genomic DNA from individual V:3 was subjected to whole exome sequencing using a 100-bp paired-end protocol on an Illumina Hi-Seq 2000 sequencer. Sequence reads obtained were aligned to the human reference sequence (GRCh37) using Bowtie2 software. The resulting alignment was processed in the SAM/BAM format using the SAMtools, Picard and GATK programs in order to correct alignments around indel sites and mark potential PCR duplicates. Following post-processing and duplicate removal, a mean depth of 64 reads was achieved for targeted exons in the homozygous regions, with 98.2% of these bases covered by at least 5 reads.

Indel and single nucleotide variants within the six candidate regions were called in the VCF format using the Unified Genotyper function of the GATK program, revealing a total of 1,847 variants. Using the dbSNP database at NCBI (http://www.ncbi.nlm.nih.gov/projects/SNP/), any variants present in dbSNP 129,

together with those variants present in dbSNP 137 with a minor allele frequency (MAF) equal to or greater than 1%, were then excluded. The 138 remaining variants were annotated using the SeattleSeq Variation Annotation server v.137 (http://snp.gs.washington.edu/SeattleSeqAnnotation137/), which identified 134 as either synonymous or deep intronic variants. Of the remaining four variants, two are present in dbSNP with a MAF <1.0%. These are rs147066399 (NM_213621:c.736C>T [p.R246W] in *HTR3A* (MIM 182139)) with a MAF of 1/4545; and rs113262393 (NM_03394.2:c.1413T>G [p.S471R] in *TANC1* (MIM 611397)) with a MAF of 9/2190. In addition, rs147066399 in *HTR3A* has been observed once in 87 South Asian samples in an in-house exome data set. A third missense variant, p.W879S in *LRP2* (NM_004525:c.2636C>G (MIM 600073)), has also been observed in heterozygous form twice in 87 South Asian samples in our in-house exome data set. Furthermore, these three variants do not segregate fully with the disease phenotype in the AI-23 family.

The remaining variant, p.P196T in *ITGB6* (NM_000888:c.586C>A) (Fig. 2A) was not present in dbSNP 137 nor in the in-house exome data set. The c.586C>A variant in *ITGB6* was further excluded in a panel of 174 control chromosomes from an ethnic diversity panel and was found to segregate perfectly with the disease phenotype in family AI-23. Both parents were heterozygous for the change. Investigation of the P196 residue, present within the I-domain of ITGB6, revealed it to be fully conserved in all orthologues and paralogues, with only ITGB8 differing at this residue (Fig. 2B), suggesting it plays a crucial role in the function of the protein. Furthermore the bioinformatic prediction packages PolyPhen2, MutationTaster, Sift, Blosum62,

Provean and MutPred consistently predicted this to be a likely pathogenic change (Supplementary Table 1).

In light of these findings we investigated a panel of 44 unrelated individuals diagnosed with hypomineralised AI from diverse backgrounds. PCR amplification and Sanger sequencing of all the coding exons and intron-exon boundaries of *ITGB6* was therefore performed. No further pathogenic variants were identified.

Enamel Phenotyping

To gain further insight into why the affected enamel undergoes premature clinical failure we undertook laboratory investigations of the remaining enamel on affected deciduous teeth and matched normal teeth. Fig. 3 shows representative μ CT buccal-lingual sections through an affected deciduous canine tooth and a matched control. The scans have been calibrated for mineral density and mapped in colour. Both teeth exhibit wear at the cusp tips where the outer covering of mineral-dense enamel has worn away to expose the less-mineralised underlying dentine. However, the affected tooth was characterised by an abnormally roughened lingual surface with areas of sub-surface enamel exhibiting reduced mineral density, though in general, affected enamel was comparable in thickness to control enamel suggesting that enamel matrix volume was not markedly affected by the mutation. The apparent subsurface voids or "holes" in the affected enamel shown in Fig. 3 are actually pits running orthogonally to the section. An orthogonal section (inset) along the plane indicated by the white dotted line reveals a typical pit running from the enamel surface towards the enamel-dentine junction. By comparison, the control tooth exhibits enamel of a more uniform

mineral density comparable to previous reports of deciduous molar enamel density which ranged from $2.69-2.92g/cm^3$ (20) and a smooth enamel surface.

At the ultrastructural level and following surface etching (Fig. 4A), SEM revealed an abnormal surface in affected teeth associated with the pits previously identified using μ CT (Fig. 4B). In control enamel (Fig. 4C), SEM of the internal enamel structure in teeth cut longitudinally along the buccal-lingual midline revealed typical enamel architecture comprising cohorts of enamel prisms changing direction relative to each other (reflecting the movement of ameloblast cohorts) to generate Hunter-Schreger banding (21). In contrast, our data suggest that prism orientation in affected enamel may be disturbed and the synchronous changes in direction of the enamel prisms responsible for generating the Hunter-Schreger bands is compromised (Fig. 4D). At the micro-scale, the structure of individual prisms in both control and affected enamel is indistinguishable using SEM (inset Figs. 4C and 4D). SEM of internal enamel structure revealed by cutting transversely through the cuspal region shows prisms in control teeth evenly arrayed across the cut surface (Fig. 4E). In contrast, affected enamel enamel exhibits areas of grossly disorganised prism architecture in the inner third of the enamel (Fig 4D).

Discussion

We identified a family of Pakistani origin segregating pitted hypomineralised AI in an autosomal recessive manner. SNP chip analysis and whole exome sequencing revealed a homozygous ITGB6 mutation resulting in the missense, p.P196T change as the only plausible cause. A screen of 44 further unrelated families revealed no further mutations indicating that this is a rare cause of AI in the cohort studied. Disruption of ITGB6 function has been linked with aged-related chronic obstructive pulmonary disease (COPD) (22). The affected individuals in the family studied are young and it is too early to know if the missense change identified will predispose them to COPD.

The integrins are a major family of cell surface-adhesion receptors involved in cellcell, cell-matrix and cell-pathogen interactions (23). Each integrin is composed of an α and β subunit which are non-covalently bound together with some promiscuity in subunit partnerships. ITGB6 commonly binds integrin- α v, forming integrin- α v β 6, an epithelial cell-specific integrin which is a predominant binder to the arginine-glycineaspartic acid (RGD) amino acid motif (24, 25). Others have described the binding of cell surface expressed integrin- α v β 6 to RGD-motifs which are widely distributed, for example in extracellular matrix proteins such as fibronectin, vitronectin and tenascin-C as well as the latency-associated peptide (LAP) of transforming growth factor- β 1 (TGF- β 1) and TGF- β 3. The missense variant identified in this study is present within the β 6-integrin I-domain, which is involved in α -integrin, divalent cation and ligand binding. Furthermore, the mutated 196P residue is in a highly conserved region next to one of the conserved extracellular cysteine residues important for integrin structure and function (Fig. 2B).

Downloaded from http://hmg.oxfordjournals.org/ at University of Leeds on December 6, 2012

Matrix-cell binding proteins such as fibronectin are important in the epithelialmesenchymal interactions during the pre-secretory stage amelogenesis (26), but are absent during the later stages (27). However the patients described herein have teeth with a near normal enamel volume, but with structurally compromised enamel, consistent with a defect that occurred after the pre-secretory phase of amelogenesis. This suggests that problems due to integrin-fibronectin RGD binding may not be the primary causal effect in the case of this mutation.

The AI phenotype in this family shares some similarity to that of mice lacking a functional allele of *Itgb6*, with both falling within the hypomineralised AI spectrum. The cause of hypomineralisation in affected teeth could be a reduction in prism density *per se* or prism density may be normal but the individual enamel crystallites within each prism may have failed to grow to their normal maximum dimensions. The laboratory phenotyping of affected human enamel presented here provides insight into why the enamel is prone to premature failure post-eruption. Although enamel of normal thickness is produced during amelogenesis of affected individuals and the normal elements of enamel architecture; i.e. enamel prisms are present, µCT and SEM indicate that the enamel is compromised by defects running from abnormal enamel surface defects (pits) towards the enamel-dentine junction. In addition, the affected teeth appear to contain localised regions of hypomineralisation; especially in the cuspal regions. There is also indication that the macro-organisation of enamel prisms in affected teeth is abnormal as evidenced by the SEM data which would be expected to impact on the mechanical properties of the enamel that depend on the organisation of prism cohorts. In normal enamel development, the synchronous movement of cohorts of ameloblasts gives rise to equivalent cohorts of prisms that

follow a sinusoidal track from the enamel-dentine junction to the enamel surface. This gives rise to the Hunter-Schreger bands which serve to inhibit crack propagation in the enamel. Based on our preliminary phenotyping we suggest that affected enamel is structurally compromised by pitting, localised hypomineralisation and disturbed prism architecture, all of which undermine the ability of the enamel to resist the stresses generated during mastication. In summary, the enamel in affected members of this family is consistent with hypomineralised AI with focal hypoplasia in the form of pits.

ITGB6 binding to latency-associated peptide (LAP) of TGF- β 1 activates the cytokine (28). TGF- β 1 and its associated receptor are expressed by secretory stage ameloblasts (autocrine signalling) and in ameloblast cell lines TGF- β 1 promotes the expression of MMP20 (29) via Runx2 (30). MMP20 is a crucial enzyme responsible for the processing of the developing enamel extracellular matrix. Failure to correctly process the enamel matrix proteins (e.g. amelogenin) would lead to retention of matrix proteins in maturing enamel and prevent the enamel mineralising fully. Retained amelogenin has been identified in other AI isoforms (31).

MMP20 has also been implicated in controlling ameloblast-ameloblast cell contact by cleaving an extracellular domain of cadherin, which in turn controls the ability of ameloblasts to execute their movements relative to each other. These movements are essential to generate the correct prism architecture (32, 33) needed to produce functional mature enamel. In MMP20 null mice normal prism decussation is abolished, matrix proteins are retained and erupting enamel undergoes rapid failure (34). Thus there is a putative molecular trail linking mutated ITGB6 to prism

disorganisation and the eruption of hypomineralised enamel (caused by retention of enamel matrix proteins) due to compromised MMP20 expression by epithelia derived ameloblasts. That Itgb6 is able to activate TGF- β 1 in oral epithelia tissue is supported by the Itgb6 mediated activation of TGF- β 1 in gingival epithelium (35). However, in argument against the hypothesis presented above, TGF- β 1 activation in mouse enamel organ, as determined by Smad1/2 phosphorylation, and MMP20 expression was similar in WT and Itgb6 knockout animals (18). It is unclear what species-species differences exist between human and mouse amelogenesis in terms of TGF- β 1 signalling and it is equally unclear how expression of ITGB6 with a missense change compares to a complete ITGB6 knockout; certainly the mouse Itgb6 knockout phenotype is different form the human example presented here as at least some degree of prism organisation is retained in affected human enamel. Clearly, more work is required to support a mechanism by which ITGB6 causes AI via a TGF- β 1 induced MMP20 activity, but we present the hypothesis as a frame work on which to base future studies.

The distribution of enamel defects in AI resulting from a mutation in ITGB6 was not evenly distributed throughout the anatomical crown. Pitting and areas of hypomineralisation were localised to the coronal portion of the tooth, the thinner cervical enamel being spared and of normal mineral density and appearance. Ameloblasts travel a shorter distance in elaborating cervical tissue and their activity takes place over a shorter time scale (as apposition rates are similar irrespective of location on the tooth) (36). Mathematical modelling has shown that the strains on ameloblasts producing enamel in the coronal region of the tooth is much greater that that experienced by their cervical counterparts, as the coronal portion of the tooth expands greatly during amelogenesis yet the numbers of ameloblasts do not increase (37). In simple terms, as coronal enamel is laid down, the surface area of the enamel increases and the monolayer sheet of ameloblasts covering the increasing surface must be able to modulate cell to cell contact to prevent stress related holes being formed in what is normally a continuous cell monolayer. Any compromise in the ability of cells to modulate their contacts with adjacent cells would leave the ameloblast monolayer more susceptible to stress induced disruption. Any holes appearing in the ameloblast monolayer during enamel secretion would be recorded in the enamel as a pit; similar to the pitting found in affected enamel in this study.

In summary, if we combine all of the information available to us from this study and the work of others we are able to suggest a hypothesis for the pathogenesis of AI in these patients (summarised in Fig. 5).

- 1. The mutation in ITGB6 would be predicted to inhibit activation of TGF β due to its failure to bind to LAP.
- 2. This in turn would inhibit expression of MMP20 which is essential for matrix processing to permit secondary crystal growth to occur. Failure to process matrix would lead to hypomineralisation as observed in our study and in the *Itgb6*-null mouse.
- 3. MMP20 is also necessary for correct ameloblast-ameloblast cell contact due to its role in cadherin processing. Failure in cell-cell contacts will compromise the ability of ameloblasts to move relative to one another, leading to the abnormal prism decussation seen here (and in the *Itgb6*-null mouse), including the disruption of Hunter-Schreger banding.

4. Mathematical modelling predicts that coronally positioned ameloblasts are under greater strain and thus the effects of any compromised cell-cell contact would be more severely manifest at the upper part of the tooth compared to the cervical margins. This corresponds to the spatial distribution of pitting that we see in the affected teeth in this study.

We propose therefore that the observed phenotype of the *ITGB6* mutation is due to the combined effects of lack of MMP20 and compromised ameloblast cell-cell binding resulting in hypomineralisation, structural abnormalities and where ameloblast strain is maximal, pitting due to the integrity of the ameloblast monolayer being compromised. Taken together these developmental defects would result in the pitted hypomineralised AI and failure of enamel function as seen in these patients.

Materials and Methods

Patients: Members of a family (AI-23), originating from Pakistan, were recruited following informed consent in accordance with the principles outlined in the declaration of Helsinki, with local ethical approval. DNA samples were obtained from family members using either Oragene[®] DNA sample collections kits (DNA Genotek, Ontario, Canada) or via venous blood samples using conventional techniques.

SNP analysis: Genomic DNAs from two affected individuals were genotyped using Affymetrix 6.0 SNP microarrays by AROS Applied Biotechnology (Aarhus, Denmark). The resulting CEL files where annotated and analysed using autoSNPa to identify shared regions of homozygosity between both affected individuals (19).

Downloaded from http://hmg.oxfordjournals.org/ at University of Leeds on December 6, 2013

Exome Sequencing: Whole exome sequencing was performed on genomic DNA using the Nextera Exome Enrichment system (Illumina, California, USA). In brief, 50ng of genomic DNA was tagged and fragmented using the Illumina Tagmentation system. Following a clean-up step, tagged DNA was PCR amplified and the subsequent library validated. Validated samples were pooled six per lane with sequencing performed on an Illumina Hi-Seq 2000 using a 100-bp paired-end protocol. Data analysis was performed using Bowtie2, SAMtools, Picard and the Genome Analysis Toolkit (GATK) (38-41).

PCR and Sequencing: Segregation of variants identified by whole exome sequencing and screening of additional AI families was performed by PCR and Sanger sequencing using standard protocols. Primers to amplify the exons and exon-intron boundaries of *ITGB6* were designed using ExonPrimer (http://ihg.gsf.de/ihg/ExonPrimer.html) and can be found in Supplementary Table 2.

Tooth Ultrastructure analysis: X-ray micro-computed tomography (μ CT) and scanning electron microscopy (SEM)

An extracted, dried AI-23 deciduous canine was compared to an extracted, dried control deciduous canine using μ CT and SEM. The control tooth was obtained with patient consent and ethical approval from a registered tissue bank operated by the School of Dentistry University of Leeds. Teeth were scanned in air together with a calibration phantom comprising a segment of mouse incisor enamel and dentine of known mineral density using a Skyscan 1172 high resolution X-ray CT scanner (Bruker, Kontich, Belgium) operated at 55kV; 10 watts power with an image pixel

size of 2-2.2µm. The teeth were rotated through 180° and shadow X-ray images captured at 0.27° intervals. The X-rays were filtered through a 0.5mm Al/Cu filter to reduce beam hardening effects. The shadow images were reconstructed using Skyscan Recon software to generate an image stack comprising sections through the teeth. The Recon software was also used to further correct ring artefacts and beam hardening. The sectional images were further analysed and using ImageJ software (National Institutes of Health, Bethesda, Maryland, USA) and calibrated with respect to mineral density using the mouse incisor as a calibrator.

For SEM, teeth were cut along the buccal-lingual midline or transversely through the cusp region with a diamond cutting disk. The cut surfaces were lightly polished using 2000 grade carborundum paper and etched for 20 seconds by gentle agitation in 30% phosphoric acid to remove any smear layer. Samples were rinsed in copious amounts of distilled water and dried under vacuum overnight prior to sputter coating with gold. SEM images were obtained using a Hitachi S-3400 operating in secondary electron emission mode at an accelerating voltage of 20kV and an emission current of 22.1µA.

Acknowledgements

The authors wish to thank the family involved in this study for their support for this research. The project was funded by the Wellcome Trust [Grant No. 093113]. J.K is supported by the NIHR Leeds Musculoskeletal Biomedical Research Unit.

Conflict of Interest

The authors declare no conflict of interest.

References

1 Bailleul-Forestier, I., Molla, M., Verloes, A. and Berdal, A. (2008) The genetic basis of inherited anomalies of the teeth. Part 1: clinical and molecular aspects of non-syndromic dental disorders. *Eur. J. Med. Genet.*, **51**, 273-291.

2 Coffield, K.D., Phillips, C., Brady, M., Roberts, M.W., Strauss, R.P. and Wright, J.T. (2005) The psychosocial impact of developmental dental defects in people with hereditary amelogenesis imperfecta. *J. Am. Dent. Assoc.*, **136**, 620-630.

3 Robinson, C., Kirkham, J., Weatherell, J.A., Richards, A., Josephsen, K. and Fejerskov, O. (1988) Mineral and protein concentrations in enamel of the developing permanent porcine dentition. *Caries. Res.*, **22**, 321-326.

4 Smith, C.E. (1998) Cellular and chemical events during enamel maturation. *Crit. Rev. Oral Biol. Med.*, **9**, 128-161.

5 Sawada, T., Yamamoto, T., Yanagisawa, T., Takuma, S., Hasegawa, H. and Watanabe, K. (1990) Evidence for uptake of basement membrane by differentiating ameloblasts in the rat incisor enamel organ. *J. Dent. Res.*, **69**, 1508-1511.

6 Porto, I.M., Merzel, J., de Sousa, F.B., Bachmann, L., Cury, J.A., Line, S.R. and Gerlach, R.F. (2009) Enamel mineralization in the absence of maturation stage ameloblasts. *Arch. Oral Biol.*, **54**, 313-321.

Lagerstrom, M., Dahl, N., Nakahori, Y., Nakagome, Y., Backman, B.,
Landegren, U. and Pettersson, U. (1991) A deletion in the amelogenin gene (AMG)
causes X-linked amelogenesis imperfecta (AIH1). *Genomics*, 10, 971-975.

8 Rajpar, M.H., Harley, K., Laing, C., Davies, R.M. and Dixon, M.J. (2001) Mutation of the gene encoding the enamel-specific protein, enamelin, causes autosomal-dominant amelogenesis imperfecta. *Hum. Mol. Genet.*, **10**, 1673-1677. 10 Kim, J.W., Simmer, J.P., Hart, T.C., Hart, P.S., Ramaswami, M.D., Bartlett, J.D. and Hu, J.C. (2005) MMP-20 mutation in autosomal recessive pigmented hypomaturation amelogenesis imperfecta. *J. Med. Genet.*, **42**, 271-275.

11 Parry, D.A., Poulter, J.A., Logan, C.V., Brookes, S.J., Jafri, H., Ferguson,

C.H., Anwari, B.M., Rashid, Y., Zhao, H., Johnson, C.A. *et al.* (2013) Identification of mutations in SLC24A4, encoding a potassium-dependent sodium/calcium exchanger, as a cause of amelogenesis imperfecta. *Am. J. Hum. Genet.*, **92**, 307-312.

12 Parry, D.A., Brookes, S.J., Logan, C.V., Poulter, J.A., El-Sayed, W., Al-

Bahlani, S., Al Harasi, S., Sayed, J., Raif el, M., Shore, R.C. *et al.* (2012) Mutations in c4orf26, encoding a Peptide with in vitro hydroxyapatite crystal nucleation and growth activity, cause amelogenesis imperfecta. *Am. J. Hum. Genet.*, **91**, 565-571.

13 Kim, J.W., Lee, S.K., Lee, Z.H., Park, J.C., Lee, K.E., Lee, M.H., Park, J.T., Seo, B.M., Hu, J.C. and Simmer, J.P. (2008) FAM83H mutations in families with autosomal-dominant hypocalcified amelogenesis imperfecta. *Am. J. Hum. Genet.*, **82**, 489-494.

14 El-Sayed, W., Parry, D.A., Shore, R.C., Ahmed, M., Jafri, H., Rashid, Y., Al-Bahlani, S., Al Harasi, S., Kirkham, J., Inglehearn, C.F. *et al.* (2009) Mutations in the beta propeller WDR72 cause autosomal-recessive hypomaturation amelogenesis imperfecta. *Am. J. Hum. Genet.*, **85**, 699-705.

15 Poulter, J.A., El-Sayed, W., Shore, R.C., Kirkham, J., Inglehearn, C.F. and Mighell, A.J. (2013) Whole-exome sequencing, without prior linkage, identifies a mutation in LAMB3 as a cause of dominant hypoplastic amelogenesis imperfecta. *Eur. J. Hum. Genet.*, in press.

Kim, J.W., Seymen, F., Lee, K.E., Ko, J., Yildirim, M., Tuna, E.B., Gencay,
K., Shin, T.J., Kyun, H.K., Simmer, J.P. *et al.* (2013) LAMB3 Mutations Causing
Autosomal-dominant Amelogenesis Imperfecta. *J. Dent. Res.*, in press.

Jonkman, M.F., Pas, H.H., Nijenhuis, M., Kloosterhuis, G. and Steege, G.
(2002) Deletion of a cytoplasmic domain of integrin beta4 causes epidermolysis
bullosa simplex. *J. Invest. Dermatol.*, **119**, 1275-1281.

Mohazab, L., Koivisto, L., Jiang, G., Kytomaki, L., Haapasalo, M., Owen,
G.R., Wiebe, C., Xie, Y., Heikinheimo, K., Yoshida, T. *et al.* (2013) Critical role for
alphavbeta6 integrin in enamel biomineralization. *J. Cell. Sci.*, **126**, 732-744.

Carr, I.M., Flintoff, K.J., Taylor, G.R., Markham, A.F. and Bonthron, D.T.
(2006) Interactive visual analysis of SNP data for rapid autozygosity mapping in consanguineous families. *Hum. Mutat.*, 27, 1041-1046.

20 Wong, F.S., Anderson, P., Fan, H. and Davis, G.R. (2004) X-ray microtomographic study of mineral concentration distribution in deciduous enamel. *Arch. Oral Biol.*, **49**, 937-944.

Lynch, C.D., O'Sullivan, V.R., Dockery, P., McGillycuddy, C.T. and Sloan,
A.J. (2010) Hunter-Schreger Band patterns in human tooth enamel. *J. Anat.*, 217, 106-115.

Morris, D.G., Huang, X., Kaminski, N., Wang, Y., Shapiro, S.D., Dolganov,
G., Glick, A. and Sheppard, D. (2003) Loss of integrin alpha(v)beta6-mediated TGFbeta activation causes Mmp12-dependent emphysema. *Nature*, 422, 169-173.

23 Zhang, K. and Chen, J. (2012) The regulation of integrin function by divalent cations. *Cell. Adh. Migr.*, **6**, 20-29.

24 Breuss, J.M., Gillett, N., Lu, L., Sheppard, D. and Pytela, R. (1993) Restricted distribution of integrin beta 6 mRNA in primate epithelial tissues. *J. Histochem. Cytochem.*, **41**, 1521-1527.

Brown, A.C., Rowe, J.A. and Barker, T.H. (2011) Guiding epithelial cell phenotypes with engineered integrin-specific recombinant fibronectin fragments. *Tissue Eng. Part A*, **17**, 139-150.

Hurmerinta, K., Kuusela, P. and Thesleff, I. (1986) The cellular origin of fibronectin in the basement membrane zone of developing tooth. *J. Embryol. Exp. Morphol.*, **95**, 73-80.

Thesleff, I., Barrach, H.J., Foidart, J.M., Vaheri, A., Pratt, R.M. and Martin, G.R. (1981) Changes in the distribution of type IV collagen, laminin, proteoglycan, and fibronectin during mouse tooth development. *Dev. Biol.*, **81**, 182-192.

Munger, J.S., Huang, X., Kawakatsu, H., Griffiths, M.J., Dalton, S.L., Wu, J., Pittet, J.F., Kaminski, N., Garat, C., Matthay, M.A. *et al.* (1999) The integrin alpha v beta 6 binds and activates latent TGF beta 1: a mechanism for regulating pulmonary inflammation and fibrosis. *Cell*, **96**, 319-328.

Gao, Y., Li, D., Han, T., Sun, Y. and Zhang, J. (2009) TGF-beta1 and
TGFBR1 are expressed in ameloblasts and promote MMP20 expression. *Anat. Rec. (Hoboken)*, **292**, 885-890.

Lee, H.K., Lee, D.S., Ryoo, H.M., Park, J.T., Park, S.J., Bae, H.S., Cho, M.I. and Park, J.C. (2010) The odontogenic ameloblast-associated protein (ODAM) cooperates with RUNX2 and modulates enamel mineralization via regulation of MMP-20. *J. Cell Biochem.*, **111**, 755-767.

31 Wright, J.T., Hall, K.I. and Yamauche, M. (1997) The enamel proteins in human amelogenesis imperfecta. *Arch. Oral Biol.*, **42**, 149-159.

32 Bartlett, J.D. and Smith, C.E. (2013) Modulation of cell-cell junctional complexes by matrix metalloproteinases. *J. Dent. Res.*, **92**, 10-17.

33 Guan, X. and Bartlett, J.D. (2013) MMP20 Modulates Cadherin Expression in Ameloblasts as Enamel Develops. *J. Dent. Res.*, in press.

Caterina, J.J., Skobe, Z., Shi, J., Ding, Y., Simmer, J.P., Birkedal-Hansen, H. and Bartlett, J.D. (2002) Enamelysin (matrix metalloproteinase 20)-deficient mice display an amelogenesis imperfecta phenotype. *J. Biol. Chem.*, **277**, 49598-49604.

Ghannad, F., Nica, D., Fulle, M.I.G., Grenier, D., Putnins, E.E., Johnston, S., Eslami, A., Koivisto, L., Jiang, G.Q., McKee, M.D. *et al.* (2008) Absence of alpha v beta 6 integrin is linked to initiation and progression of periodontal disease. *Am. J. Pathol.*, **172**, 1271-1286.

Robinson, C. and Kirkham, J. (1984) Is the Rat Incisor Typical? *INSERM*,
125, 377-386.

37 Cox, B. (2010) A multi-scale, discrete-cell simulation of organogenesis: Application to the effects of strain stimulus on collective cell behavior during ameloblast migration. *J. Theor. Biol.*, **262**, 58-72.

Langmead, B. and Salzberg, S.L. (2012) Fast gapped-read alignment withBowtie 2. *Nat. Methods*, 9, 357-359.

Li, H., Handsaker, B., Wysoker, A., Fennell, T., Ruan, J., Homer, N., Marth,
G., Abecasis, G. and Durbin, R. (2009) The Sequence Alignment/Map format and
SAMtools. *Bioinformatics*, 25, 2078-2079.

40 McKenna, A., Hanna, M., Banks, E., Sivachenko, A., Cibulskis, K., Kernytsky, A., Garimella, K., Altshuler, D., Gabriel, S., Daly, M. *et al.* (2010) The Genome Analysis Toolkit: a MapReduce framework for analyzing next-generation DNA sequencing data. *Genome Res.*, **20**, 1297-1303. 41 DePristo, M.A., Banks, E., Poplin, R., Garimella, K.V., Maguire, J.R., Hartl, C., Philippakis, A.A., del Angel, G., Rivas, M.A., Hanna, M. *et al.* (2011) A framework for variation discovery and genotyping using next-generation DNA sequencing data. *Nat. Genet.*, **43**, 491-498.

Legends to Figures

Figure 1. Family pedigree and clinical dental phenotypes for AI-23. (A) Pedigree of family AI-23 recording the three affected individuals within a consanguineous family. DNA was available for all labelled individuals. (B) (i & ii) The clinical appearances for V8 aged 7-years of the early mixed dentition with premature enamel failure. Surface enamel pitting is evident on many teeth including the partially erupted permanent lower incisors (arrows) and via the 'speckled black' appearances due to exogenous staining in the pits. Inset image is a higher magnification image of the deciduous tooth (arrow *) highlighting the pitting. The retention of enamel over the cusps of the permanent molar teeth (arrow heads) at this stage highlights the dramatic loss of enamel from the rest of the dental crown, even though these teeth have been in the mouth for a short period of time. (iii) Clinical appearances of the upper dentition for V3 aged 9-years illustrating how the enamel can fracture cleanly away leaving a shoulder of remaining enamel at the cervical margin (arrows). The enamel of the newly erupted second permanent molar teeth has yet to fail (arrow *). (iv) Dental radiograph of V3 aged 7-years confirming a near-normal enamel volume in the unerupted 2nd premolar (arrowhead) and 2nd molar (arrowhead +) lower permanent teeth with a clear difference in radiodensity between enamel and dentine, consistent with what is observed in normal teeth. The 1st lower permanent molar tooth has been restored with a metal crown (+). The crown of the permanent lower 3rd molar tooth is starting to mineralise (arrowhead *).

Figure 2. Electropherogram of mutation and conservation of the P196T variant.

(A) Representative electropherogram of the ITGB6 mutation in an affected member of family AI-23 alongside the wild-type sequence. Arrows indicate the localisation of

25

the variant. **(B)** Conservation of the P196 residue in orthologues (upper) and paralogues (lower). Conserved residues are highlighted. Human (NP_000879), Chimp (XP_001149234), Macaca (XP_001094740), Dog (XP_857148), Cat (XP_003990848), Horse (XP_001492914), African Elephant (XP_003406050), Wild Boar (NP_001090892), Cow (NP_777123), Guinea Pig (XP_003478725), Sheep (NP_001107244), Rat (NP_001004263), Mouse (NP_067334), Chicken (XP_422037), Zebra Finch (XP_002193421), Frog (NP_001090775), Zebrafish (XP_003199474), Human ITGB1 (NP_596867), ITGB2 (NP_001120963), ITGB3 (NP_000203), ITGB4 (NP_000204), ITGB5 (NP_002204), ITGB7 (NP_000880) and ITGB8 (NP_002205).

Figure 3. Phenotypic analyses of enamel: µCT

(A) μ CT confirmed a reasonable enamel volume in affected teeth, but with multiple enamel surface and sub-surface abnormalities. Particularly striking were the regions of enamel exhibiting reduced mineral density and pits running for the enamel surface deep in to the bulk of the enamel.

Figure 4. Phenotypic analyses of enamel: SEM

(A) SEM of etched control enamel surface showed the characteristic appearance of arrays of enamel prisms terminating at the surface. (B) In contast, the affected enamel was punctured by numerous pits and the prism array was more obscure. (C) SEM of the internal prim architecture of control enamel in longitudinal section revealed the characteristic sinusoidal pattern of prism cohorts giving rise to Hunter–Schreger bands. (D) The prism architecture in affected enamel was less regular and clear Hunter-Schreger bands were less distinct. The inset images in (C) and (D) show that individual prism structure at the micron level in control and affected enamel is indistinguishable by SEM in some areas. (E) SEM of transversely cut sections through control cuspal enamel showed the characteristic array of prisms themselves in transverse section (higher magnification inset). (F) In affected enamel the inner enamel layer is structurally abnormal with loss of prism organisation. Structural features designed to provide mechanical stability that depend on the correct interrelationship between prism cohorts (e.g. Hunter-Schreger bands) will be compromised in this enamel (inset shows higher magnification detail).

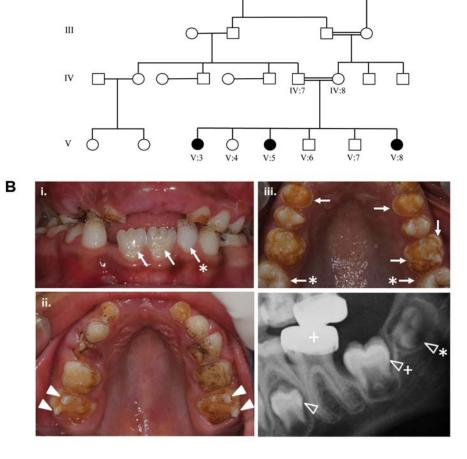
Figure 5. Cartoon summarising the hypothesis presented here to explain the mechanism underpinning the AI subtype described. (A) At the beginning of normal enamel secretion an army of ameloblasts, present as a monolayer, migrates away from the preformed dentine surface leaving enamel matix in their wake. (B) As the cuspal enamel volume increases the ameloblasts modulate cell-cell contacts to cope with the stresses encountered by the monolayer being required to cover an ever expanding area. We hypothesise that ITGB6 upregulates MMP20 expression (via TGFβ activation). This in turn cleaves cadherin thus allowing ameloblasts to modulate cell-cell contacts to cope with the increasing stress of an expanding enamel surface and to allow cohorts of ameloblast to move relative to one another to produce sinusoidal prism architecture. MMP20 also processes enamel matrix proteins which is required for their final degradation prior to the completion of mineralisation. In affected enamel we hypothesise that cadherin cleavage and matrix processing are compromised due to the ITGB6 mutation resulting in breaks in the ameloblast monolayer in the cuspal regions leading to pitting, abnormal prism architecture and retained matrix proteins that inhibit final enamel mineralisation.

27

Region	Size (Mb)	Variants not in dbSNP 129 or MAF ≤ 1%	and predicted functional	and segregates with the disease
Chr2:154,600,940-173,240,770	18.64Mb	31	3	1
Chr7:154,812,233-157,683,557	2.87Mb	4	0	-
Chr10:80,853,408-90,425,474	9.57Mb	8	0	-
Chr11:100,244,686-113,840,625	13.60Mb	21	1	0
Chr12:4,023,387-21,726,294	17.70Mb	41	0	-
Chr22:22,798,234-33,658,203	10.86Mb	33	0	-
Total	72.6Mb	138	4	1

Table 1: Summary of variants in AI-23 candidate disease regions and variants discovered by exome sequencing. The total variants identified in each

region are shown.

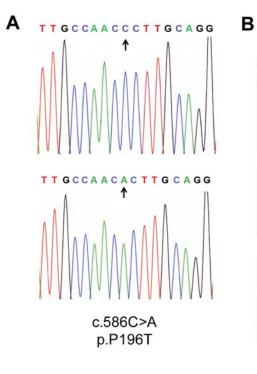


Α

I

П

29



	p.P196T				
		\downarrow			
Human	181	PVSPFVKTTPEEIANPCSSIPYFCLPTFGFK	211		
Chimp	181	PVSPFVKTTPEEIANPCSSIPYFCLPTFGFK	211		
Macaca	181	PVSPFVKTTPEEIANPCSSIPYFCLPTFGFK	211		
Dog	201	PVSPFVKTTPEEIANPCSSIPYFCLPTFGFK	231		
Cat	201	PVSPFMKTTPEEIANPCSSIPYFCLPTFGFK	231		
Horse	201	PVSPFMKTSPEEIANPCSSIPYFCLPTFGFK	231		
Elephant	181	PVSPFMKTTPEEIANPCSSIPYFCLPTFGFK	211		
Wild Boar	181	PISPFMKTTPEEIANPCSSIPYFCLPTFGFK	211		
Cow	181	PISPFMKTTPEEIANPCSSIPYFCLPTFGFK	211		
Guinea Pig	181	PVSPFMKTTPEEIANPCSSIPYICLPTFGFK	211		
Sheep	181	P ISPFMKTTPEE I ANPCSS I PYFCLPTFGFK	211		
Rat	181	PVSPFMKTTPEEITNPCSSIPYFCLPTFGFK	211		
Mouse	181	PVSPFMKTTPEEITNPCSSIPYFCLPTFGFK	211		
Chicken	181	PVSPFIKTTAEEINNPCRSVPYECLPTFGYK	211		
Zebra Finch	181	PVSPFIKTTAAEINNPCRSVPYECLPTFGYK	211		
Frog	181	PVSPF1KTVPKD1ENPCHS1PYYCLPTFGYK	211		
Zebrafish	177	PVLPFIKITREELANPCRSFDLECLPTFGYR	207		
ITGB6	182	VSPFVKTTP-EEIANPCSSIPYFCLPTFG	209		
ITGB1	191	VMPYISTTP-AKLRNPCTS-EQNCTSPFS	218		
ITGB2	176	VLPFVNTHP-DKLRNPCPNKEKECOPPFA	203		
ITGB3	187	VSPYMYISPPEALENPCYDMKTTCLPMFG	215		
ITGB4	179	SVPQTDMRP-EKLKEPWPNSDPPFS	202		
ITGB5	187	ISPFSYTAP-RYQTNPCIGYKLFPNCVPSFG	216		
ITGB7	201	VLPFVSTVP-SKLRHPCPTRLERCOSPFS	228		
ITGB8	196	VSPYISIHP-ERIHNQCSDYNLDCMPPHG	223		

30

